JOURNAL OF GUIDANCE, CONTROL, AND DYNAMICS
Vol. 18, No. 5, September–October 1995

Near-Minimum-Time Eigenaxis Rotation Maneuvers Using Reaction Wheels

Willem H. Steyn*
University of Stellenbosch, Stellenbosch 7600, South Africa

A near-minimum-time (near-maximum-acceleration/deceleration) control technique is presented to rotate a spacecraft around its eigenaxis (shortest angular path). Practical control constraints such as wheel torque and wheel speed are also taken into account. In this paper a nominally nadir pointing satellite in a circular low Earth orbit under passive gravity gradient stabilization and active reaction wheel control will be used as an example. A standard linear feedback quaternion regulator will be used to three-axis stabilize the spacecraft before and after each large angular rotation. Robustness against inertia modeling errors is ensured by tracking the reference maneuver. The algorithm presented can easily be adapted to be used on inertially stabilized spacecraft.

Introduction

REMOTE sensing satellites often have to embark on minimum-time large-slew maneuvers to point their payload (e.g., body-fixed cameras) at different targets within a short span of time. This problem has already been addressed by various researchers in the past: Wie et al.[1] proposed a linear quaternion feedback regulator with open-loop decoupling control torque for gyroscopic forces to ensure eigenaxis rotations. Reaction wheel speed constraints were however not considered; it was assumed that the rotation will be slow enough, resulting in no violation of the wheel saturation limits. Van den Bosch et al.[2] presented an adaptive control method to enable the Infrared Astronomical Satellite to track a linear reference model around an eigenaxis. Although reaction wheel constraints were considered in their proposed algorithm, model updating was needed to ensure only near eigenaxis rotation and the rotation time was not minimized. Both these papers only developed and applied their algorithms to inertially stabilized spacecraft.

D'Amario and Stubbs[3] designed a single-rotation-axis (eigenaxis) autopilot for rapid attitude maneuvers on spacecraft using jet thrusters. Premaneuver calculations are done to obtain a staircase time history of the commanded eigenaxis angular acceleration/deceleration. The calculations ensure that at least one thruster will be on near full time (near maximum acceleration and deceleration) except during coasting when a maximum rotation speed limit is reached. Only gyroscopic coupling nonlinearities were considered in their autopilot model. Although the autopilot commands were computed open loop, rate feedback tracking was provided during the maneuver.

Redding and Adams[4] described fuel-optimal jet thruster maneuvers for the Space Shuttle. Linearized dynamics is assumed and a two-point boundary value problem solved in real time. The solution provides open-loop jet firing commands and setpoints for standard autopilot feedback loops. Angular rate limits are satisfied by adopting a fixed-end-time formulation and by the correct choice of the final time.

Vadali[5] used the principles of variable structure control theory to implement robust large-angle maneuvers on a spacecraft. Initially maximum torque is used to reach a sliding manifold; then the state trajectory is controlled to slide on the manifold toward the target attitude. The sliding motion was chosen to be optimal in the sense of a quadratic performance index in the Euler parameters and angular velocities. Although the maneuvers were not time optimal, they were robust against modeling errors and disturbance torques.

Li and Bainum[6] presented an iterative numerical approach to find the minimum slew time and the corresponding optimal controls of a general rigid spacecraft. Bilimoria and Wie[7] described a time-optimal three-axis reorientation method for a rigid spacecraft. They showed that in general the eigenaxis rotation maneuver is not time optimal. Reductions in the slew time of a symmetric body compared to eigenaxis rotations of less than 10% were obtained during simulations. However, this was achieved at the expense of a substantial increase in control energy (each actuator per axis is commanded simultaneously in a full bang-bang manner). Their algorithm was exclusively derived for an inertially symmetric (e.g., spherical or cubical) rigid body.

Byers and Vadali[8] extended the time-optimal reorientation problem by presenting approximate solutions to the switching times for nonsymmetric rigid bodies. A feedforward/feedback control law to approximate the time-optimal solution was also proposed. This control law took care of modeling errors caused by gyroscopic coupling and differences in moment of inertia. However, the algorithms in Ref. 8 are computationally very demanding. Both Refs. 7 and 8 demonstrated a marginal decrease in rotation time compared to an eigenaxis rotation at the expense of a substantial increase in control energy.

The algorithm presented in this paper attempts to balance the opposing goals of minimum time and minimum control effort when using reaction wheels. A practical solution to these opposing goals might be to minimize the maneuver time around the eigenaxis. An eigenaxis rotation results in the shortest angular path and therefore also in near-minimum control effort during minimum-time maneuvers. The unique constant ratio properties of the Euler vector components and body angular rates during an eigenaxis rotation are used to design a computational undemanding algorithm for real-time implementation. Reaction wheel torque and speed limitations are also explicitly satisfied by the algorithm. Rate feedback tracking is used during the eigenaxis rotations to minimize any perturbations that might be caused by modeling errors (especially inertia uncertainty) and external disturbances.

Only three orthogonally mounted reaction wheels are assumed in this paper. However, the NASA standard configuration[9] with an extra skew reaction wheel can also be used. The required three-element control torque vector must then be transformed by any suitable transformation matrix to a four-element wheel vector. Likewise, the reaction wheel speed and torque saturation constraints must be inversely transformed to the three-element vector values as used in the newly proposed algorithm. Momentum dumping is not considered within the scope of this paper. It is assumed that a suitable dumping mechanism is implemented to ensure small values of wheel angular momentum before the slew maneuver commences.

Received April 28, 1994; revision received Jan. 27, 1995; accepted for publication Jan. 27, 1995.

*Senior Lecturer, Department of Electrical and Electronic Engineering.

Preliminaries

Dynamic Equations

The dynamics of a spacecraft in inertial space are governed by Euler's equations of motion. With the added influence of the gravity

gradient boom and reaction wheel moments the equation can be expressed in vector form as

$$\boldsymbol{I}\dot{\boldsymbol{\omega}}_B^I = \boldsymbol{N}_{gg} + \boldsymbol{N}_d + \boldsymbol{N}_{\text{gyro}} - \boldsymbol{N}_{\text{wheel}} \tag{1}$$

where

$$\boldsymbol{N}_{\text{gyro}} = -\boldsymbol{\omega}_B^I \times \left(\boldsymbol{I}\boldsymbol{\omega}_B^I + \boldsymbol{h}\right)$$

$$\boldsymbol{N}_{gg} = 3\omega_o^2\left[\boldsymbol{z}_o^B \times \boldsymbol{I}\boldsymbol{z}_o^B\right]$$

is the gravity gradient torque vector,

$$\boldsymbol{N}_{\text{wheel}} = \dot{\boldsymbol{h}}$$

is the reaction wheel torque, and

$$\boldsymbol{\omega}_B^I = [\omega_x \quad \omega_y \quad \omega_z]^T$$

is the inertially referenced angular body rate vector. Here, $\boldsymbol{I}$ is the inertia matrix of the spacecraft, ω_o the orbital angular rate, $\boldsymbol{z}_o^B$ the nadir unit vector along the body reference axes, $\boldsymbol{h}$ the reaction wheel angular momentum, and $\boldsymbol{N}_d$ the disturbance torque vector.

Kinematic Equations

The kinematics (attitude) of the satellite will be modeled making use of quaternions. A quaternion model does not suffer from any singularities, no trigonometric functions are needed in the transformation matrix, and it can easily be referenced to the orbit-following coordinate system. The orbit and body coordinate sets for a nominally nadir pointing satellite is defined as shown in Fig. 1. The parameterization of the quaternion vector is done as

$$\begin{aligned} q_1 &\equiv e_{xo}\sin\left(\tfrac{1}{2}\Phi\right) \qquad q_2 \equiv e_{yo}\sin\left(\tfrac{1}{2}\Phi\right) \\ q_3 &\equiv e_{zo}\sin\left(\tfrac{1}{2}\Phi\right) \qquad q_4 \equiv \cos\left(\tfrac{1}{2}\Phi\right) \end{aligned} \tag{2}$$

where e_{xo}, e_{yo}, e_{zo} are the components of the Euler vector in orbit-referenced coordinates and Φ is the rotation angle around the Euler vector (eigenaxis). The kinematics can be updated by the following vector set of differential equations:

$$\dot{\boldsymbol{q}} = \tfrac{1}{2}\boldsymbol{\Omega}\boldsymbol{q} \tag{3}$$

with

$$\boldsymbol{\Omega} = \begin{bmatrix} 0 & \omega_{zo} & -\omega_{yo} & \omega_{xo} \\ -\omega_{zo} & 0 & \omega_{xo} & \omega_{yo} \\ \omega_{yo} & -\omega_{xo} & 0 & \omega_{zo} \\ -\omega_{xo} & -\omega_{yo} & -\omega_{zo} & 0 \end{bmatrix}$$

where

$$\boldsymbol{\omega}_B^O = [\omega_{xo} \quad \omega_{yo} \quad \omega_{zo}]^T$$

is the orbit-referenced angular body rate vector. The transformation matrix to transform any vector from orbital to body-referenced coordinates can be written in quaternion format as

$$\boldsymbol{A} = \begin{bmatrix} q_1^2 - q_2^2 - q_3^2 + q_4^2 & 2(q_1q_2 + q_3q_4) & 2(q_1q_3 - q_2q_4) \\ 2(q_1q_2 - q_3q_4) & -q_1^2 + q_2^2 - q_3^2 + q_4^2 & 2(q_2q_3 + q_1q_4) \\ 2(q_1q_3 + q_2q_4) & 2(q_2q_3 - q_1q_4) & -q_1^2 - q_2^2 + q_3^2 + q_4^2 \end{bmatrix} \tag{4}$$

The angular body rates referenced to the orbit-following coordinates can be obtained from the inertially referenced body rates by using the transformation matrix in Eq. (4):

$$\boldsymbol{\omega}_B^O = \boldsymbol{\omega}_B^I - \boldsymbol{A}[0 \quad -\omega_o \quad 0]^T = \boldsymbol{\omega}_B^I + \omega_o\boldsymbol{A}_2 \tag{5}$$

Error Quaternion

Whenever quaternions are used directly in the control laws of any attitude control algorithms, it is convenient to define the error quaternion as the quaternion difference between the current quaternion and the commanded quaternion. The error quaternion can be calculated from the latter two sets of quaternions by using the definition of quaternion division:

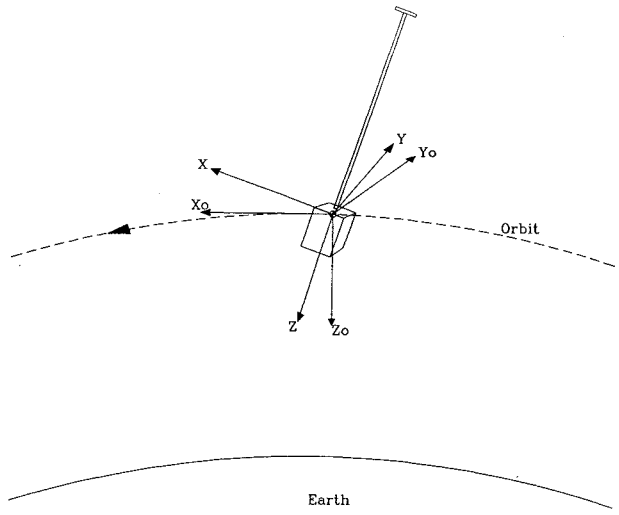

Fig. 1 Orbit and body coordinate sets.

$$\begin{bmatrix} q_{1e} \\ q_{2e} \\ q_{3e} \\ q_{4e} \end{bmatrix} = \begin{bmatrix} q_{4c} & q_{3c} & -q_{2c} & -q_{1c} \\ -q_{3c} & q_{4c} & q_{1c} & -q_{2c} \\ q_{2c} & -q_{1c} & q_{4c} & -q_{3c} \\ q_{1c} & q_{2c} & q_{3c} & q_{4c} \end{bmatrix} \begin{bmatrix} q_1 \\ q_2 \\ q_3 \\ q_4 \end{bmatrix} \tag{6}$$

where q_{ie} are the components of the error quaternion, q_{ic} the components of the commanded quaternion, and q_i the components of the current orbit-referenced quaternion. Whenever the current quaternion and the commanded quaternion coincide ($\boldsymbol{q} = \boldsymbol{q}_c$), the error quaternion $\boldsymbol{q}_e = [0\ 0\ 0\ 1]^T$.

Eigenaxis Maneuver

During an eigenaxis slew the rotation axis ($\boldsymbol{e} = [e_{xo}\ e_{yo}\ e_{zo}]^T$) stays constant with respect to the orbital reference frame for a nadir pointing satellite. Then for the vector components of the error quaternion

$$\frac{q_{ie}(t)}{q_{je}(t)} = \text{const} \qquad i, j = 1, 2, 3, \qquad i \neq j \tag{7}$$

Likewise, during the eigenaxis maneuver the angular body rate vector (orbit referenced) will point in the same direction as the Euler axis:

$$\boldsymbol{\omega}_B^O = [e_{xo}\dot{\Phi} \quad e_{yo}\dot{\Phi} \quad e_{zo}\dot{\Phi}]^T = [\omega_{xo} \quad \omega_{yo} \quad \omega_{zo}]^T \tag{8}$$

Thus,

$$\frac{\omega_{io}(t)}{\omega_{jo}(t)} = \text{const} \qquad i, j = x, y, z, \qquad i \neq j \tag{9}$$

If we assume relatively small gyroscopic, gravity gradient, and disturbance torques compared to the maximum reaction wheel torque during a slew maneuver, a near-minimum-time eigenaxis rotation would be possible when (see Fig. 2)

$$\ddot{\Phi}(t) = \begin{cases} +a & \{t \in t_0, t_h\} \\ -a & \{t \in t_h, t_f\} \end{cases} \tag{10}$$

where a is the near maximum acceleration/deceleration possible with reaction wheels, t_h the time to reach the halfway mark during

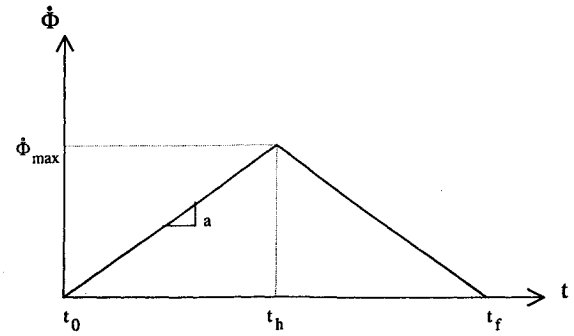

Fig. 2 Angular rate during minimum-time eigenaxis rotation without wheel speed limiting.

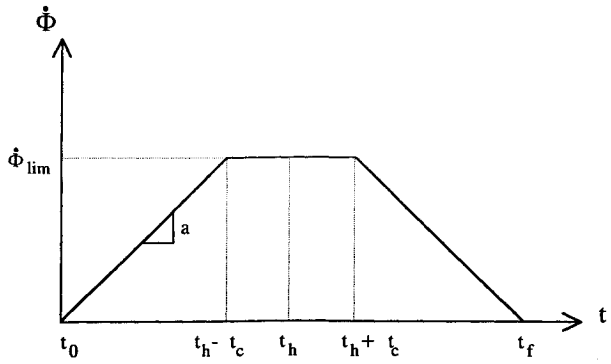

Fig. 3 Angular rate during minimum-time eigenaxis rotation with wheel speed limiting.

the slew maneuver, and $t_f = 2t_h$ the time to complete the slew maneuver. If the wheel speed limit is reached during the acceleration phase, further acceleration has to be stopped and the satellite must be allowed to coast until the appropriate time to enter the deceleration phase. The rule to follow is to ensure equal periods of time (t_c) before and after the halfway mark during the coasting phase (see Fig. 3).

From Eq. (8) it is clear that the angular body rates ω_{xo}, ω_{yo}, and ω_{zo} will have similar shapes to Figs. 2 and 3 but with slopes $\pm e_{xo}a$, $\pm e_{yo}a$, and $\pm e_{zo}a$, respectively. A linear increase/decrease in the angular body rates can be obtained by a large constant acceleration/deceleration slew torque from the reaction wheels. A small (compared to the slew torque) additional wheel torque must be added to the slew torque to keep the satellite's rotation around the eigenaxis, as can be seen from Eqs. (11) and (12). By using Eqs. (1) and (5), we obtain the orbit-referenced dynamic equation

$$\begin{aligned} I\dot{\omega}_B^O &= N_{gg} + N_d + N_{\text{gyro}} - N_{\text{wheel}} + \omega_o I\dot{A}_2 \\ &= N_{\text{slew}} + N_d \end{aligned} \tag{11}$$

The total reaction wheel torque can then be taken as (ignoring wheel friction)

$$N_{\text{wheel}} = I_w\dot{\omega}_w = \dot{h} = N_{\text{add}} - N_{\text{slew}} \tag{12}$$

with

$$N_{\text{add}} = N_{gg} + N_{\text{gyro}} + \omega_o I\dot{A}_2 \tag{13}$$

The assumption of a relatively small additional torque will be true if the gyroscopic torque is small, as the gravity gradient torque and the last term in Eq. (13) (a torque to keep the satellite nominally nadir pointing) have small magnitude. A small gyroscopic torque will occur if the spacecraft is three-axis stabilized with low reaction wheel momentum before the eigenaxis rotation commences. This can be ensured by a suitable momentum dumping method. Therefore, the satellite has a small total angular momentum initially.

If we ignore the disturbance torque as being small (compared to the reaction wheel slew torque) and assume $I = \text{diag}(I_X, I_Y, I_Z)$, we have, during the acceleration and deceleration phases of the slew maneuver,

$$\frac{I_i\dot{\omega}_{io}}{I_j\dot{\omega}_{jo}} = \frac{N_{\text{wheel-}i}}{N_{\text{wheel-}j}}\bigg|_{\text{slew}} = \text{const} \qquad i, j = x, y, z, \qquad i \neq j \tag{14}$$

We already have, from Eqs. (7–9), e.g., when $i = x$ and $j = y$, during an eigenaxis slew,

$$\omega_{xo}/\omega_{yo} = e_{xo}/e_{yo} = q_{1e}/q_{2e}$$

Thus,

$$\frac{N_{\text{wheel-}x}}{N_{\text{wheel-}y}}\bigg|_{\text{slew}} = \frac{I_X q_{1e}}{I_Y q_{2e}} \tag{15}$$

Relationship (15) (in all combinations of x, y, z and q_{1e}, q_{2e}, q_{3e}) can now be used at the start of an eigenaxis slew to determine the respective reaction wheel slew torques during acceleration and deceleration. The slew torque can then be written as

$$N_{\text{slew}} = \begin{cases} +s \min_i \left|\dfrac{N_{\text{sat-}1}}{I_i q_{ie}}\right| \text{diag}(\boldsymbol{I})\boldsymbol{q}_{\text{vec}} & t \in (0, t_h - t_c) \\ \mathbf{0} & t \in (t_h - t_c, t_h + t_c) \\ -s \min_i \left|\dfrac{N_{\text{sat-}i}}{I_i q_{ie}}\right| \text{diag}(\boldsymbol{I})\boldsymbol{q}_{\text{vec}} & t \in (t_h + t_c, 2t_h) \end{cases} \tag{16}$$

where $\boldsymbol{q}_{\text{vec}} = [q_{1e}\ q_{2e}\ q_{3e}]^T$, $N_{\text{sat-}i}$ is the saturated wheel torque in body axis i, and $s \in (0, 1)$ is the amount of total saturated torque used for the maneuver. To satisfy the torque constraint on the reaction wheels, the wheel with the saturated slew torque requirement [i from Eq. (16)] will be fixed to slightly less than the maximum limit, i.e., $s < 1$. This is done to enable a near-minimum-time slew while providing for the small additional torques as explained above.

Although the actual reaction wheel control torque (12) is computed during the maneuver in an open-loop manner, the halfway mark is determined using feedback from the error quaternion. The largest error quaternion vector component [$q_{1e}(t)$, $q_{2e}(t)$, or $q_{3e}(t)$] is compared to its precomputed value at the halfway mark (q_{half}):

$$\max_i |q_{ie}(t)| - q_{\text{half}} = \begin{cases} >0 & \forall t < t_h \\ <0 & \forall t > t_h \end{cases} \tag{17}$$

where

$$q_{\text{half}} = \frac{\max_i |q_{ie}(t_0)|}{|\sin(\Phi/2)|}\left|\sin\left(\frac{\Phi}{4}\right)\right| \tag{18}$$

The full algorithm for a near-time-optimal eigenaxis rotation can be summarized as follows:

1) Determine the initial error quaternion $\boldsymbol{q}_e(t_0)$ from Eq. (6).

2) Compute the respective x, y, and z axis reaction wheel slew torques from Eq. (16).

3) Use Eq. (18) to obtain q_{half} for the dominant torque axis error quaternion vector component.

4) Use the acceleration phase slew torques plus the additional torques (13) to compute the total amount of wheel torque to be applied to each wheel.

5) Apply these torques and repeat step 4 until $t > t_h$ using Eq. (17), then go to step 8, or until one of the wheel speeds approach its limit (say 95% of maximum to provide for the additional torques during the coasting phase), then go to step 6.

6) If a wheel speed limit is encountered, zero all the wheel slew torques and apply only the additional torques during a coasting phase.

7) Repeat step 6 until an equal coasting period t_c is completed before and after the halfway mark, then go to step 8.

8) Use the deceleration phase slew torques plus the additional torques (13) to compute the total amount of wheel torque to be applied to each wheel.

9) Apply these torques and repeat step 8 until $t = 2t_h = t_f$.

To compensate for any small attitude and rate errors at the completion of the eigenaxis rotation due to unmodeled disturbances or

small inertia mismatches, a standard[1,10] linear quaternion feedback regulator will be used:

$$N_{\text{wheel}} = K q_{\text{vec}} + D\omega_B^O \tag{19}$$

Wie et al.[1] proved, using Lyapunov functions, that global stability is guaranteed if $K^{-1}D$ is positive definite. A suitable choice can be $K = k\mathbf{1}$ and $D = d\mathbf{1}$ (where $\mathbf{1}$ = identity matrix), with k and d positive constants. As proven by Wie et al.,[1] this choice for K leads to global stability and robustness against inertia uncertainty. It was also shown in Ref. 1 that an eigenaxis rotation will occur when $K = kI$ (where I = inertia matrix) and when the additional torques N_{add} from Eq. (13) are added to Eq. (19), but the rotation will not be time optimal.

In case of larger inertia mismatches, greater deviations can occur from the eigenaxis during the rotation. A feedback compensation torque using the measured body angular rate components (referenced to the orbit-following coordinates) can solve this problem. The constant ratio property of the angular body rate components (9) during an eigenaxis rotation will be used to formulate a feedback controller tracking the reference rate.

The feedback torque will be taken as proportional to the difference between a reference angular rate vector and the measured angular rate vector. The feedback rate-tracking torque to be added to the total wheel torque (12) is

$$N_{\text{comp}} = C\left[\omega_B^O - \omega_{\text{ref}}\right] \tag{20}$$

where

$$I\dot{\omega}_{\text{ref}} = N_{\text{slew}} \tag{21}$$

In the next section near eigenaxis convergence and stability of the rate tracking control law (20), in spite of inertia mismatches, will be proven. As will be shown, convergence stability will be achieved whenever C is larger than a certain minimum diagonal positive matrix.

Eigenaxis Convergence

Let I_n denote the nominal value of the inertia matrix and ΔI the uncertainty. Therefore $I = I_n + \Delta I$. Then from Eq. (1) using I and Eqs. (12) and (13) using I_n, it follows that

$$(I_n + \Delta I)\dot{\omega}_B^I = 3\omega_o^2\left[z_o^B \times \Delta I z_o^B\right] - \omega_B^I \times \Delta I \omega_B^I - \omega_o I_n \dot{A}_2 + N_{\text{slew}} \tag{22}$$

or in terms of the orbit-referenced body angular rates (11),

$$(I_n + \Delta I)\dot{\omega}_B^O = 3\omega_o^2\left[z_o^B \times \Delta I z_o^B\right] - \omega_B^I \times \Delta I \omega_B^I - \omega_o \Delta I \dot{A}_2 + N_{\text{slew}} \tag{23}$$

If we assume that the orbit angular rate ω_o is much smaller than the body angular rate components during the slew maneuver, 1) $\omega_B^I \approx \omega_B^O$ and 2) the first and third terms on the right-hand side of Eq. (23) can be ignored. For an axially symmetric spacecraft (diagonal inertia matrix), Eq. (23) can then be approximated as

$$\begin{aligned}
\dot{\omega}_{xo} &\approx \frac{\Delta I_Y - \Delta I_Z}{I_X + \Delta I_X}\omega_{yo}\omega_{zo} - \frac{\Delta I_X}{I_X + \Delta I_X}\eta_{\text{slew-}x} + \eta_{\text{slew-}x} \\
\dot{\omega}_{yo} &\approx \frac{\Delta I_Z - \Delta I_X}{I_Y + \Delta I_Y}\omega_{xo}\omega_{zo} - \frac{\Delta I_Y}{I_Y + \Delta I_Y}\eta_{\text{slew-}y} + \eta_{\text{slew-}y} \\
\dot{\omega}_{zo} &\approx \frac{\Delta I_X - \Delta I_Y}{I_Z + \Delta I_Z}\omega_{xo}\omega_{yo} - \frac{\Delta I_Z}{I_Z + \Delta I_Z}\eta_{\text{slew-}z} + \eta_{\text{slew-}z}
\end{aligned} \tag{24}$$

where

$$\eta_{\text{slew}} = \begin{cases} +s \min\limits_i \left|\dfrac{N_{\text{sat-}i}}{I_i q_{ie}}\right| q_{\text{vec}} & \text{for acceleration phase} \\ \mathbf{0} & \text{for coasting phase} \\ -s \min\limits_i \left|\dfrac{N_{\text{sat-}i}}{I_i q_{ie}}\right| q_{\text{vec}} & \text{for deceleration phase} \end{cases} \tag{25}$$

The first two terms on the right-hand side of Eq. (24) will be the main cause of perturbations from the eigenaxis due to inertia mismatches. The last term will be the normalized slew torque needed for a true eigenaxis rotation. If we take the body angular rate components as the sum of an eigenaxis reference component and a perturbational component,

$$\omega_B^O = \omega_{\text{ref}} + \Delta\omega \qquad \dot{\omega}_{\text{ref}} = \eta_{\text{slew}}$$

Then using Eq. (24) and subtracting (adding to wheel torque) the normalized feedback torque of Eq. (20), the perturbational dynamics becomes ($C = \text{diag}[C_X\ C_Y\ C_Z]$)

$$\begin{aligned}
&\begin{bmatrix} I_X + \Delta I_X & 0 & 0 \\ 0 & I_Y + \Delta I_Y & 0 \\ 0 & 0 & I_Z + \Delta I_Z \end{bmatrix} \Delta\dot{\omega} \\
&= \begin{bmatrix} -C_X & k_1\omega_{\text{ref-}z} & k_1\omega_{\text{ref-}y} \\ k_2\omega_{\text{ref-}z} & -C_Y & k_2\omega_{\text{ref-}x} \\ k_3\omega_{\text{ref-}y} & k_3\omega_{\text{ref-}x} & -C_Z \end{bmatrix} \Delta\omega \\
&+ \begin{bmatrix} k_1(\Delta\omega_y\Delta\omega_z + \omega_{\text{ref-}y}\omega_{\text{ref-}z}) \\ k_2(\Delta\omega_x\Delta\omega_z + \omega_{\text{ref-}x}\omega_{\text{ref-}z}) \\ k_3(\Delta\omega_x\Delta\omega_y + \omega_{\text{ref-}x}\omega_{\text{ref-}y}) \end{bmatrix} \\
&- \begin{bmatrix} \Delta I_X & 0 & 0 \\ 0 & \Delta I_Y & 0 \\ 0 & 0 & \Delta I_Z \end{bmatrix} \eta_{\text{slew}}
\end{aligned} \tag{26}$$

where

$$k_1 = \Delta I_Y - \Delta I_Z \qquad k_2 = \Delta I_Z - \Delta I_X \qquad k_3 = \Delta I_X - \Delta I_Y$$

In Eq. (26), $k_1, \ldots, k_3$ are small constants depending only on the inertia uncertainty, with the property that they can never all have the same sign. The eigenaxis reference angular rate components increase linearly with time during the acceleration phase, stay constant during a coasting phase, or decrease linearly with time during the deceleration phase. The dynamics of Eq. (26) will be stable if the time-varying system matrix of $\Delta\omega$ have stable eigenvalues. It can easily be shown by applying Routh's stability criterion to the characteristic equation of the system that a sufficient condition for stable eigenvalues will be

$$\begin{aligned}
C_X &> \max\{|k_1\omega_{\text{ref-}y}|, |k_1\omega_{\text{ref-}z}|\} \\
C_Y &> \max\{|k_2\omega_{\text{ref-}x}|, |k_2\omega_{\text{ref-}z}|\} \\
C_Z &> \max\{|k_3\omega_{\text{ref-}x}|, |k_3\omega_{\text{ref-}y}|\}
\end{aligned} \tag{27}$$

There is a limit to the size of the time-varying forcing terms in Eq. (26) due to the wheel speed and torque constraints. Their influence on $\Delta\omega$ can be reduced further by increasing the positive constants C_X, C_Y, and C_Z; this will speed up convergence and reduce tracking errors to the eigenaxis. The simple rate tracking control law of Eq. (20) will therefore result in stable feedback with arbitrary small perturbations from the eigenaxis due to inertia modeling errors.

Simulation Results

A small cubical microsatellite of 50 kg with a gravity gradient boom of 4 m and tip mass deployed along the nominal zenith ($-Z_0$ axis) direction, will be used to test the new algorithm. This structure gives a moment of inertia (MOI) tensor $I = \text{diag}(40, 40, 2)$ kgm^2. The orbit configuration will be circular and sun synchronous at an altitude of 800 km. Three identical reaction wheels with a wheel MOI $I_w = 5\times10^{-4}$ kgm^2, a maximum wheel torque $N_{\text{sat}} = 4\times10^{-3}$ N-m, and a maximum wheel speed of 4800 rpm will be used.

To compare the various simulations all the rotations will be done from a stable nadir pointing attitude to a certain 1–2–3 Euler attitude of roll, pitch, and yaw. The satellite is then kept at the specific pointing attitude for a while and finally commanded back toward

Table 1 Comparison between new algorithm and quaternion regulator

Roll, deg	Pitch, deg	Yaw, deg	Slew time, %	Integrated wheel, torque,%
50	−70	90	+1.0	+46.6
20	−10	−60	+29.9	−19.4
−10	10	0	+68.0	−85.5
80	0	0	+1.0	+1.0
0	0	175	+83.9	−52.5

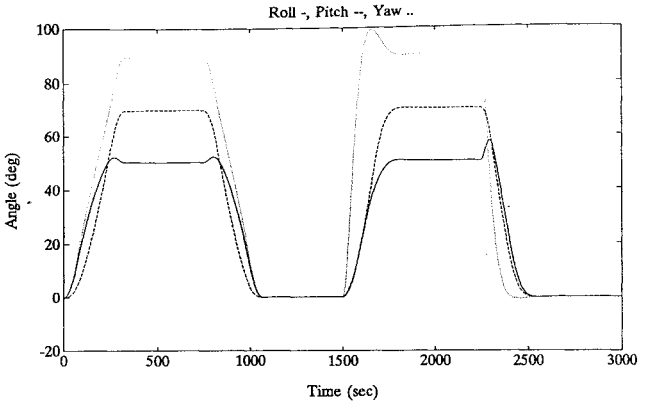

Fig. 4 Euler angles for large angular slew (new and Q regulator).

nadir. The new algorithm is compared to an eigenaxis quaternion feedforward/feedback regulator[1]:

$$N_{\text{wheel}} = kIq_{\text{vec}} + dI\omega_B^Q + N_{\text{add}} \tag{28}$$

Equation (28) will ensure eigenaxis rotations when not subjected to the wheel speed and wheel torque constraints as proven by Wie et al.[1] In these simulations, however, saturation of wheel speed and torque can occur during certain large angular slew maneuvers. Gain values for $k = 0.00175$ and $d = 0.05$ were used. These values for k and d were arrived at through simulation optimization, the criteria being to minimize the slew time of large slew maneuvers.

Table 1 lists some typical simulation results. The average slew time and time-integrated torque values between the new algorithm and the quaternion regulator are compared. A positive value presents the improvement due to the new algorithm and a negative value the opposite. The new algorithm outperforms the quaternion regulator with respect to the slew time in all cases, although not by much when speed and torque saturation of the quaternion regulator occur. The torque saturations normally lead to a decrease in energy effectiveness when compared to the new algorithm. As expected, an unsaturated quaternion regulator (small angular or yaw rotations) also delivers eigenaxis rotations. These rotations are slower but more energy efficient compared to the new algorithm.

Figure 4 shows a large angular rotation with the corresponding roll, pitch, and yaw angles during the maneuvers. Initially the new near-minimum-time eigenaxis algorithm is used and at time 1500 s the quaternion feedforward/feedback regulator is employed. A more symmetric behavior and pitch, roll, and yaw angles that reach their target values simultaneously are observed for the new algorithm. Although the slew times were almost identical (approximately 300 s), the new eigenaxis rotation results in almost 50% less control effort due to the saturation and non–eigenaxis rotation when using the quaternion regulator (see Figs. 6 and 7).

Figure 5 shows the corresponding reaction wheel angular momentum. [Note: The angular rate is expressed in revolutions per orbit (rpo) units.] The effect of the wheel constraints can be noticed: The maximum slope of the angular momentum is limited by the wheel torque constraint. The magnitude of the angular momentum is also limited to within the maximum wheel momentum of ± 240 kgm^2· rpo. The wheel speed is limited to this maximum value by zeroing of the corresponding wheel torque of the quaternion regulator. The coasting phase is entered at ± 228 kgm^2· rpo (5% lower

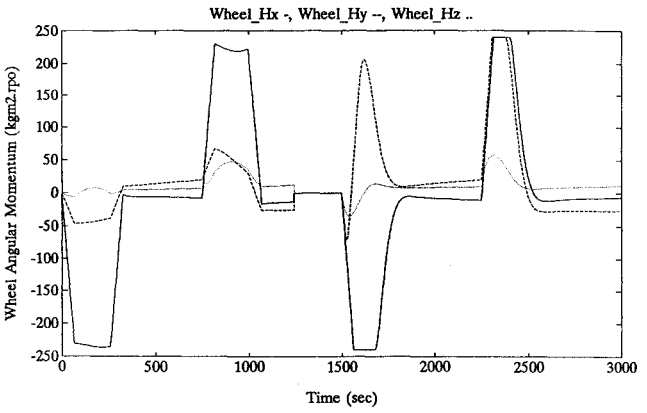

Fig. 5 Reaction wheel angular momentum during large slew (new and Q regulator).

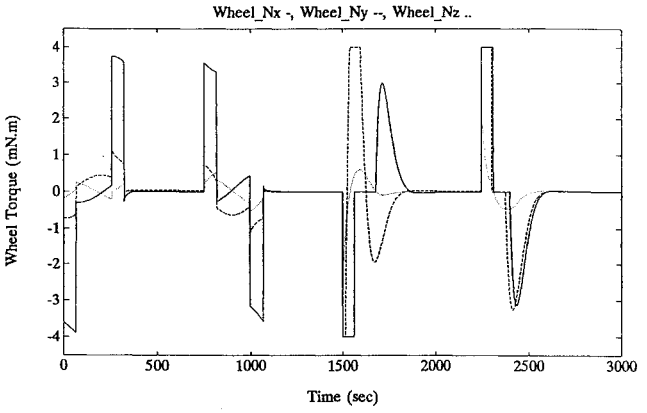

Fig. 6 Reaction wheel torques during large slew (new and Q regulator).

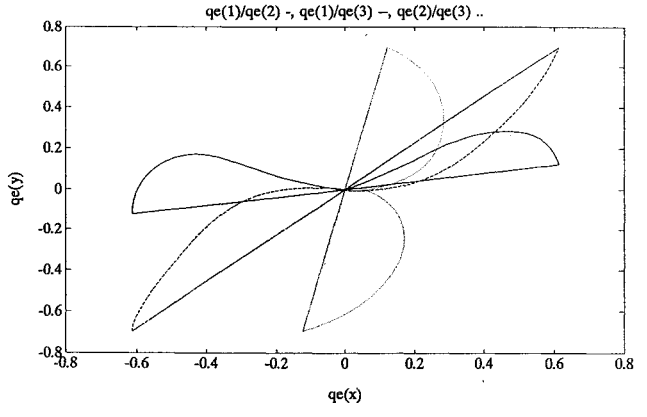

Fig. 7 Error quaternion ratio plots during large slew (new and Q regulator).

than maximum) for the newly proposed algorithm to provide for the additional torque influence during this phase.

Figure 6 shows the corresponding reaction wheel torques. It can clearly be seen from the integrated area under these curves that the eigenaxis rotation results in less control effort. The maximum wheel torque constraint of $\pm 4 \times 10^{-3}$ N-m is also adhered to by saturation torque limiting of the linear feedback regulator. The new eigenaxis algorithm satisfies the torque constraint by using 3.6×10^{-3} N-m [$s = 0.9$ in Eq. (16)] as the upper limit on the wheel slew torque, therefore providing 0.4×10^{-3} N-m for the additional small torques.

Figure 7 shows the corresponding behavior of the error quaternion vector components. The straight lines in Fig. 7 indicate the pure eigenaxis rotation (constant ratios in the error quaternion vector components) of the new method. The large excursions from the straight lines indicate the non-eigenaxis rotation of the quaternion regulator. Figure 8 shows a smaller angular rotation when the quaternion regulator also delivers an eigenaxis maneuver. The slew time improvement from the new algorithm is now clearly observable.

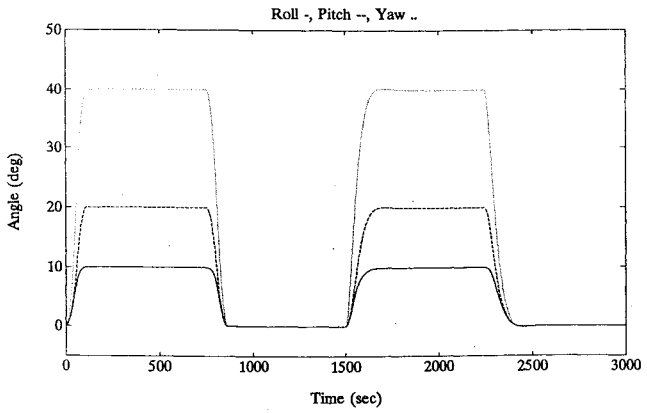

Fig. 8 Euler angles during small angular slew (new and Q regulator).

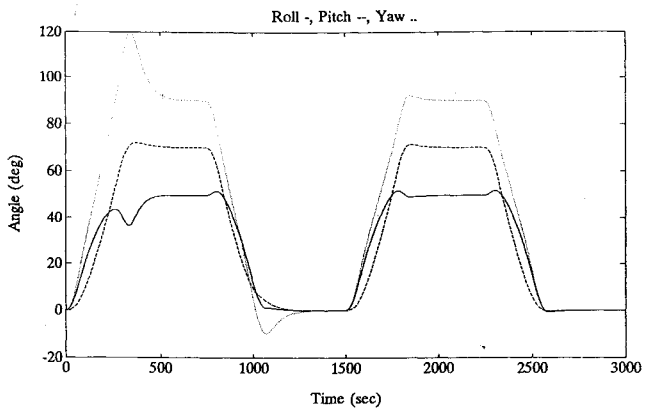

Fig. 9 Euler angles during large angular slew with 10% MOI mismatch.

Figure 9 presents the same angular maneuver as in Fig. 4, but this time with ±10% modeling errors in the MOI values of the satellite: $I_n = \text{diag}(44, 44, 1.8)$ kgm^2. The first part (until 1500 s) shows the rotations using the new controller, but without the feedback rate-tracking torque. Undercompensation in roll and overcompensation in yaw are clearly visible. The attitude and rate errors are then corrected at the end of the rotation by a linear quaternion feedback regulator. The latter part of the simulation demonstrates the effect when the feedback rate tracker is added. The roll, pitch, and yaw angles are almost identical to the ideally modeled case of Fig. 4.

Conclusions

A practical, near-minimum-time, eigenaxis rotational method is proposed for a three-axis reaction wheel and gravity gradient stabilized nadir pointing satellite. This method considers all of the important constraints of reaction wheels. The new algorithm can be described as an open-loop one-switch bang-bang (or bang-off-bang) controller with feedback tracking of the reference rate. Compared to a simulation optimized quaternion feedforward/feedback regulator, the new method improved the slew time performance for all of the target rotations investigated. The control energy performance for large angular slew maneuvers also improved compared to the quaternion regulator, owing to output torque saturation. Unmodeled disturbances and MOI errors can degrade the overall performance of the new controller to some extent, due to the open-loop computational method of the reaction wheel torque. Disturbance torques will normally be a few orders of magnitude smaller than the near-maximum reaction wheel torque employed during the rotation. These disturbances will therefore not cause significant deviations from the eigenaxis in the limited time of a slew maneuver.

The main cause for degradation can be from MOI modeling mismatches. Simulations indicated that modeling errors of less than 5% still result in near eigenaxis rotations. For larger MOI mismatches a feedback rate tracker can be utilized to minimize any large deviations from the eigenaxis. The stability of the closed-loop system with this addition was also proven.

References

[1]Wie, B., Weiss, H., and Arapostathis, A., "Quaternion Feedback Regulator for Spacecraft Eigenaxis Rotations," *Journal of Guidance, Control, and Dynamics*, Vol. 12, No. 3, 1989, pp. 375–380.

[2]Van den Bosch, P. P. J., Jongkind, W., and Van Swieten, A. C. M., "Adaptive Attitude Control for Large-Angle Slew Manoeuvres," *Automatica*, Vol. 22, No. 2, 1986, pp. 209–215.

[3]D'Amario, L. A., and Stubbs, G. S., "A New Single-Rotation-Axis Autopilot for Rapid Spacecraft Attitude Maneuvers," *Journal of Guidance, Control, and Dynamics*, Vol. 2, No. 4, 1979, pp. 339–346.

[4]Redding, D. C., and Adams, N. J., "Optimized Rotation-Axis Attitude Maneuver Controller for the Space Shuttle Orbiter," *Journal of Guidance, Control, and Dynamics*, Vol. 10, No. 1, 1987, pp. 4–13.

[5]Vadali, S. R., "Variable-Structure Control of Spacecraft Large-Angle Maneuvers," *Journal of Guidance, Control, and Dynamics*, Vol. 9, No. 2, 1986, pp. 235–239.

[6]Li, F., and Bainum, P. M., "Numerical Approach for Solving Rigid Spacecraft Minimum Time Attitude Maneuvers," *Journal of Guidance, Control, and Dynamics*, Vol. 13, No. 1, 1990, pp. 38–43.

[7]Bilimoria, K. D., and Wie, B., "Time Optimal Three-Axis Reorientation of a Rigid Spacecraft," *Journal of Guidance, Control, and Dynamics*, Vol. 16, No. 3, 1993, pp. 446–452.

[8]Byers, R. M., and Vadali, S. R., "Quasi-Closed-Form Solution to the Time-Optimal Rigid Spacecraft Reorientation Problem," *Journal of Guidance, Control, and Dynamics*, Vol. 16, No. 3, 1993, pp. 453–461.

[9]Vadali, S. R., and Junkins, J. L., "Optimal Open-Loop and Stable Feedback Control of Rigid Spacecraft Attitude Maneuvers," *Journal of the Astronautical Sciences*, Vol. 32, No. 2, 1984, pp. 105–122.

[10]Wie, B., and Barba, P. M., "Quaternion Feedback for Spacecraft Large Angle Maneuvers," *Journal of Guidance, Control, and Dynamics*, Vol. 8, No. 3, 1985, pp. 360–365.